JACS
JOURNAL OF THE AMERICAN CHEMICAL SOCIETY
Article
pubs.acs.org/JACS

Direct Observation of Transient Surface Species during Ge Nanowire Growth and Their Influence on Growth Stability

Saujan V. Sivaram, Naechul Shin,[†] Li-Wei Chou, and Michael A. Filler*

School of Chemical & Biomolecular Engineering, Georgia Institute of Technology, Atlanta, Georgia 30332, United States

Supporting Information

ABSTRACT: Surface adsorbates are well-established choreographers of material synthesis, but the presence and impact of these short-lived species on semiconductor nanowire growth are largely unknown. Here, we use infrared spectroscopy to directly observe surface adsorbates, hydrogen atoms and methyl groups, chemisorbed to the nanowire sidewall and show they are essential for the stable growth of Ge nanowires via the vapor−liquid−solid mechanism. We quantitatively determine the surface coverage of hydrogen atoms during nanowire growth by comparing ν(Ge−H) absorption bands from *operando* measurements (i.e., during growth) to those after saturating the nanowire sidewall with hydrogen atoms. This method provides sub-monolayer chemical information at relevant reaction conditions while accounting for the heterogeneity of sidewall surface sites and their evolution during elongation. Our findings demonstrate that changes to surface bonding are critical to understand Ge nanowire synthesis and provide new guidelines for rationally selecting catalysts, forming heterostructures, and controlling dopant profiles.

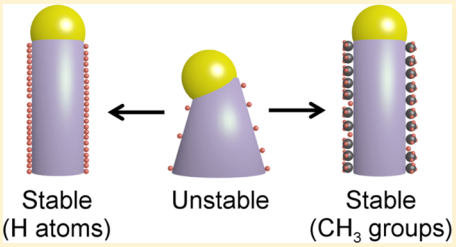

INTRODUCTION

Semiconductor nanowires are emerging as indispensable nanoscale building blocks for next generation energy conversion, electronic, and photonic devices.[1−3] The vapor−liquid−solid (VLS) mechanism—whereby a liquid eutectic "catalyst" droplet collects precursor molecules (or atoms) from the vapor and directs crystallization of the solid nanowire—is a ubiquitous method for bottom-up nanowire synthesis. The ability to encode functionalities along the nanowire length, via modulation of the vapor phase composition and/or temperature during growth, enables pn junctions,[4] heterostructures,[5] and even twinning superlattices.[6] However, catalyst instabilities,[7−9] radial dopant gradients,[10,11] or kinking[12,13] are equally common. Such observations demonstrate that the mechanistic understanding of growth remains insufficient for the *a priori* control of nanowire structure and function.

The conventional belief is that short-lived surface adsorbates may have some influence on semiconductor nanowire growth, and thus structure,[14−16] but are nonessential actors. For example, the surface-bound hydrogen atoms generated upon the heterogeneous decomposition of conventional hydride precursors are assumed, by analogy to thin film deposition, to rapidly desorb.[17] However, this assumption may not hold for nanowire synthesis since the catalyst droplet enables growth at conditions distinct from those used for thin films.[18] Identifying, quantifying, and understanding the impact of surface adsorbates, whose bonding and concentration are likely distinct during and after growth, requires measurements at reaction conditions (i.e., *operando*). The situation is further complicated for nanowires due to the heterogeneity of sidewall facets and evolution of total surface sites as the nanowire elongates. Notably, *operando* transmission electron microscopy has successfully probed catalyst phase transitions,[19] trijunction oscillations,[20,21] and defect formation,[22] but it cannot access chemical bonding.

We use infrared spectroscopy, as illustrated in Figure 1A, to show the importance of sidewall (i.e., solid−vapor interface) chemistry for the growth of Au-catalyzed Ge nanowires. We find that covalently bonded surface hydrogen atoms, reactive intermediates in the heterogeneous decomposition of Ge_2H_6, suppress taper by impeding Ge_2H_6 adsorption and, quite unexpectedly, must be present above a critical coverage to sustain growth. The delivery of methyl groups to the nanowire sidewall via GeH_3CH_3 chemisorption enables stable elongation even at conditions where surface hydrogen coverage is low. Our work demonstrates that surface chemistry can strongly influence nanowire growth, provides methods to overcome limits imposed by conventional hydride-based precursors, and suggests new chemical strategies for the *a priori* synthesis of complex nanowire structures.

RESULTS

Nanowire Growth and Observation of Surface Hydrogen. Arrays of Ge nanowires are synthesized in an ultrahigh vacuum chamber coupled to an infrared spectrometer (see Experimental Section and Figure S1). A thin layer of Au is deposited on a vacuum-prepared Ge(111) substrate, which is then heated in the presence of Ge_2H_6 (20% in He) to grow single-crystalline, ⟨111⟩-oriented Ge nanowires. We employ a two-step growth procedure, including "incubation" and

Received: April 13, 2015
Published: July 6, 2015

DOI: 10.1021/jacs.5b03818
J. Am. Chem. Soc. 2015, 137, 9861−9869

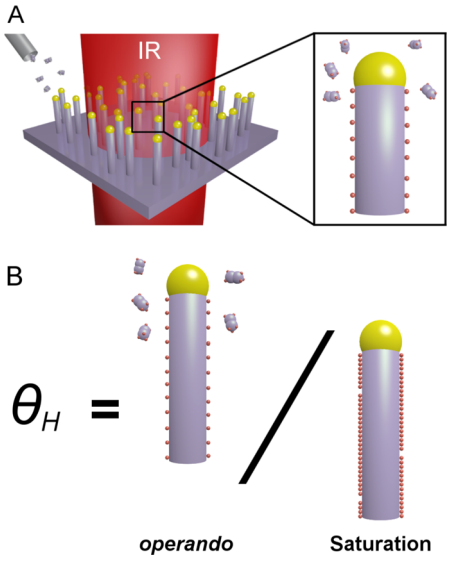

Figure 1. Measuring nanowire sidewall surface chemistry and quantitatively determining hydrogen coverage. (A) Illustration of *operando* transmission infrared spectroscopy for a nanowire ensemble. Magnified image shows hydrogen atoms bonded to the nanowire sidewall during Ge_2H_6 exposure. Purple and red spheres represent Ge and H atoms, respectively. Purple cylinders represent the Ge nanowires and the AuGe eutectic catalyst is shaded in gold. (B) Surface hydrogen coverage, θ_H, is determined by comparing the amount of surface hydrogen bonded to the nanowire during growth (*operando*) and after cooling to saturate the surface (saturation).

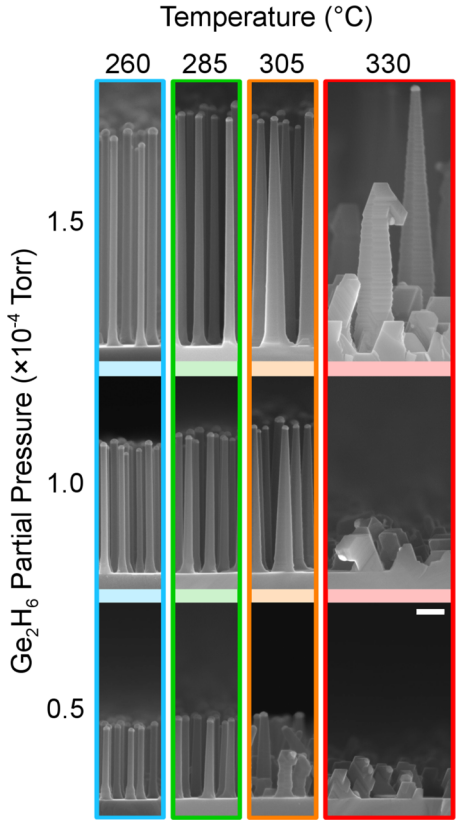

Figure 2. Evolution of nanowire morphology. Representative side-view SEM images showing Ge nanowire morphology as a function of T_{sub} and $p_{Ge_2H_6}$ after elongation for 40 min. All images are measured along the ⟨110⟩ direction. Scale bar, 200 nm.

"elongation", to ensure narrow nanowire diameter and areal density distributions (see Figures S2 and S3). On the basis of the elongation temperature (260−330 °C), axial nanowire growth rates (10−35 nm/min), and catalyst shape (see Figure S4), we infer that growth occurs via the subeutectic VLS mechanism which has been well documented for Au-catalyzed Ge nanowires heated above the eutectic temperature (T_e = 361 °C).[19]

We observe the onset of a growth instability as substrate temperature (T_{sub}) increases. Figure 2 shows this behavior and that it does not depend on a single growth parameter, since unstable growth begins closer to T_{sub} = 305 and 330 °C in the low-pressure ($p_{Ge_2H_6}$ = 0.5 × 10^{-4} Torr) and high-pressure ($p_{Ge_2H_6}$ = 1.5 × 10^{-4} Torr) regimes, respectively. Surprisingly, this departure from stable growth occurs at temperatures closer to T_e, where the catalyst is expected to be more liquid-like.

During nanowire growth, we probe the vibrational modes of surface hydrogen atoms on the sidewall with *operando* transmission infrared spectroscopy. The ν(Ge−H) stretching features appearing between 1960 and 2000 cm^{-1} in Figure 3 confirm the presence of chemisorbed hydrogen atoms, which exist as reactive intermediates prior to recombinatively desorbing as H_2.[23] This surface hydrogen must originate from dissociative adsorption of Ge_2H_6 since He is the sole carrier gas. Consistent with expectations, only monohydride is detectable at the temperatures examined here.[24] The presence of multiple peaks results from hydrogen adsorbed on different sidewall facets (see Figure S4). Below ∼330 °C, we find that ν(Ge−H) absorption intensity increases monotonically for stable growth at steady state and attribute this trend to the increasing sidewall surface area as the nanowire elongates. At ∼330 °C, ν(Ge−H) peak intensity suddenly decreases.

Method To Determine Sidewall Hydrogen Coverage.

From our measurements, we determine a time- and sidewall area-averaged surface hydrogen coverage (θ_H) to quantitatively show the connection between nanowire surface chemistry and growth behavior. To calculate θ_H, we extract quantities proportional to the number of hydrogen-covered and total sidewall surface sites from infrared spectra recorded during growth (i.e., *operando*) and after cooling to room temperature in Ge_2H_6 to saturate the surface with hydrogen atoms, respectively. The calculation of θ_H is illustrated in Figure 1B and mathematically described via eq 1:

$$\theta_H = \frac{I^{norm}_{operando}}{I^{norm}_{saturation}} = \frac{\int A^{norm}_{operando}(\tilde{\nu})\, d\tilde{\nu}}{\int A^{norm}_{saturation}(\tilde{\nu})\, d\tilde{\nu}} \quad (1)$$

where $I^{norm}_{operando}$ is the ν(Ge−H) integrated peak intensity determined from normalized (*vide infra*) *operando* spectra, $A^{norm}_{operando}(\tilde{\nu})$; $I^{norm}_{saturation}$ is the ν(Ge−H) integrated peak intensity determined from normalized postgrowth saturation spectra, $A^{norm}_{saturation}(\tilde{\nu})$; and $\tilde{\nu}$ is frequency in wavenumbers.

As-recorded absorption spectra for each T_{sub} and $p_{Ge_2H_6}$ combination must be normalized to take into account (i) differences in nanowire areal density, and thus total nanowire surface area, (ii) the temperature dependence of ν(Ge−H) absorption strength, and (iii) the use of different backgrounds for *operando* and postgrowth saturation spectra. The normalized spectra, $A^{norm}_{operando}(\tilde{\nu})$ and $A^{norm}_{saturation}(\tilde{\nu})$, are obtained via:

DOI: 10.1021/jacs.5b03818
J. Am. Chem. Soc. 2015, 137, 9861−9869

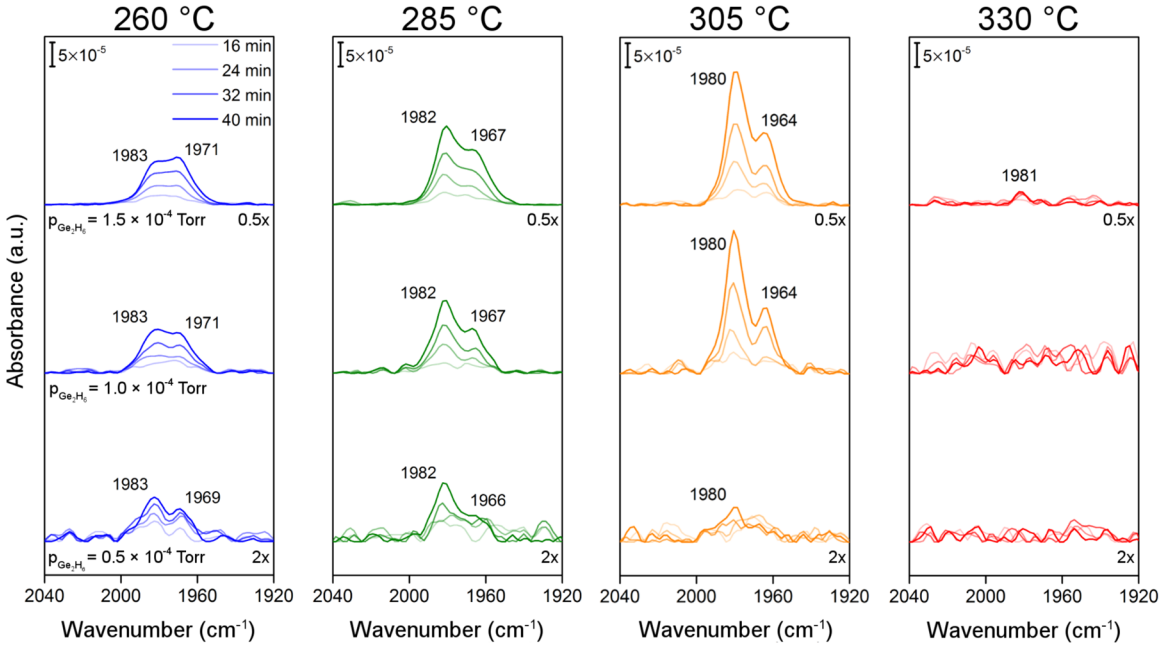

Figure 3. Evolution ν(Ge−H) stretching modes during nanowire elongation. Time-dependent *operando* transmission infrared spectra collected during elongation at the indicated T_{sub} and $p_{Ge_2H_6}$. Spectra for $p_{Ge_2H_6}$ = 0.5 and 1.5 × 10^{-4} Torr are scaled by a factor of 2 and 0.5, respectively, for ease of comparison. All background spectra are of the initial 8 min of nanowire elongation at the same T_{sub} and $p_{Ge_2H_6}$. The 40 min spectra at all conditions are used for $A_{operando_{40\ min}}(\tilde{\nu})$. All spectra are recorded with the substrate oriented perpendicular to the beam path (see Figure 1A).

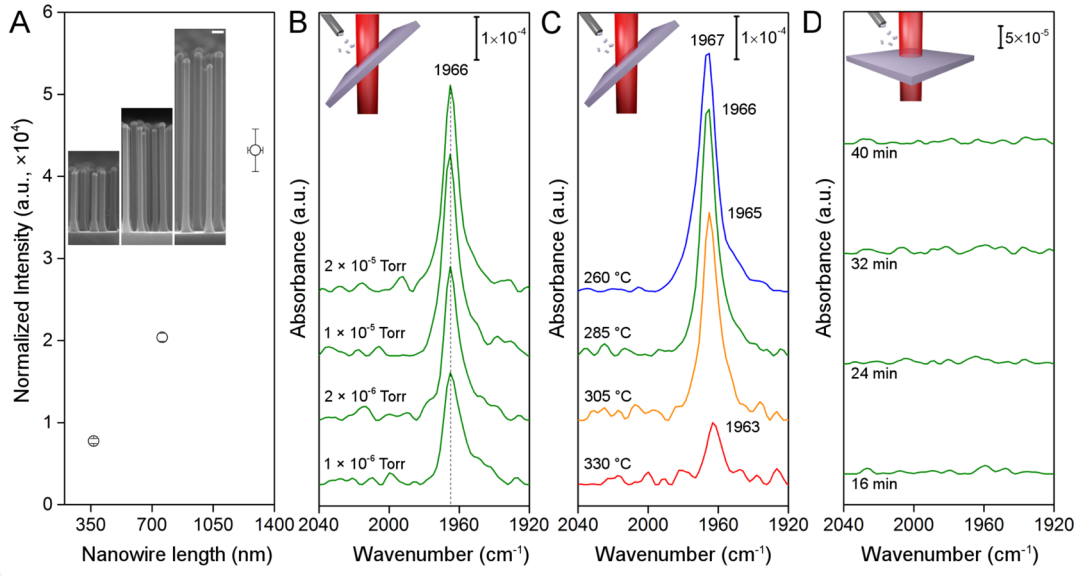

Figure 4. Validation of Beer−Lambert law, constant oscillator strength, and nanowire sidewall measurement. (A) Normalized integrated peak intensity of the final *operando* spectra for untapered nanowires elongated at T_{sub} = 260 °C and $p_{Ge_2H_6}$ = 0.5 − 1.5 × 10^{-4} Torr (from Figure 3) plotted with respect to average nanowire length. Average length determined from 50 nanowires per sample. Inset: SEM images (from Figure 2) show increasing nanowire length with no taper. Scale bar, 200 nm. (B) *Operando* infrared absorption spectra of the ν(Ge−H) stretching region for a Au-free Ge(111) substrate oriented 65° relative to the infrared beam path at T_{sub} = 285 °C as a function of $p_{Ge_2H_6}$. The dotted line is a guide to show that the peak position is constant. Background spectra are of the initial vacuum-prepared, Au-free Ge(111) substrate maintained at T_{sub} = 285 °C. (C) *Operando* infrared absorption spectra of the ν(Ge−H) stretching region for a Au-free Ge(111) substrate exposed to a saturation $p_{Ge_2H_6}$ as a function of T_{sub}. Background spectra are of the initial vacuum-prepared, Au-free Ge(111) substrate maintained at the corresponding T_{sub}. (D) Time-dependent *operando* infrared absorption spectra of a Au-free Ge(111) substrate oriented perpendicular to the infrared beam path and exposed to $p_{Ge_2H_6}$ = 1 × 10^{-4} Torr at T_{sub} = 285 °C. All background spectra are of the initial vacuum-prepared, Au-free Ge(111) substrate maintained at T_{sub} = 285 °C in vacuum. The absence of ν(Ge−H) features at all times confirms the substrate does not contribute to the nanowire spectra (e.g., Figure 3).

DOI: 10.1021/jacs.5b03818
J. Am. Chem. Soc. 2015, 137, 9861−9869

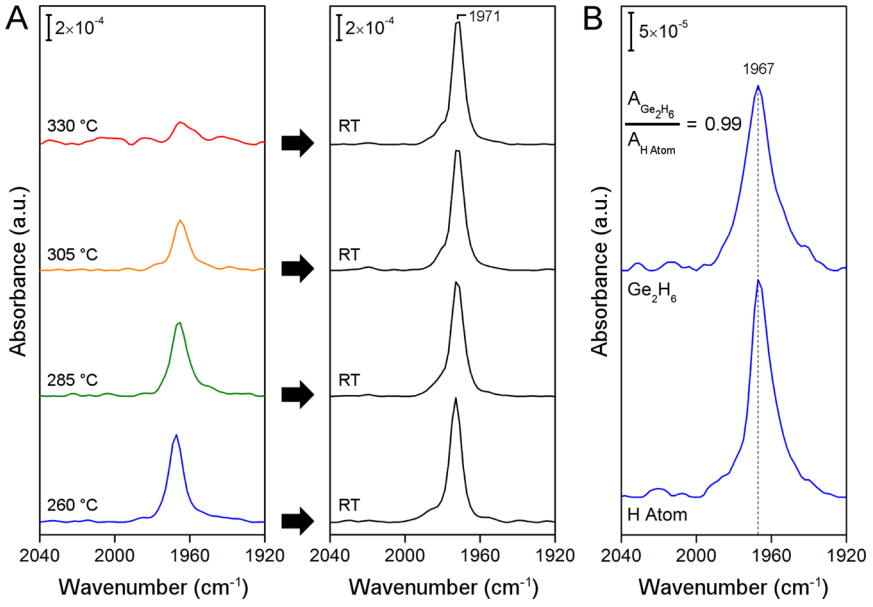

Figure 5. Postgrowth saturation method valid for all elongation temperatures and proportional to absolute number of surface sites. (A, left) *Operando* infrared absorption spectra of the ν(Ge−H) stretching region for a Au-free Ge(111) substrate oriented 65° relative to the infrared beam path at the indicated T_{sub} and $p_{Ge_2H_6}$ = 1 × 10^{-4} Torr. All background spectra are of the initial vacuum-prepared, Au-free Ge(111) substrate maintained at the indicated T_{sub}. (A, right) Postgrowth saturation infrared absorption spectra of the ν(Ge−H) stretching region recorded after cooling the substrate to room temperature at $p_{Ge_2H_6}$ = 1 × 10^{-4} Torr. Background spectra are of the initial vacuum-prepared, Au-free Ge(111) substrate maintained at room temperature. These data confirm that cooling to room temperature in Ge_2H_6 from all elongation temperatures results in a surface saturated with hydrogen atoms. (B) *Operando* infrared absorption spectra of the ν(Ge−H) stretching region for a Au-free Ge(111) substrate oriented 58° relative to the infrared beam path at T_{sub} = 260 °C after saturation exposures of Ge_2H_6 and H atoms. Background spectra are of the initial vacuum-prepared, Au-free Ge(111) substrate maintained at T_{sub} = 260 °C. The ratio of these integrated peak intensities is 0.99, confirming that saturation with Ge_2H_6 adsorption yields a complete monolayer.

$$A^{norm}_{operando}(\tilde{\nu}) = \frac{A_{operando_{40min}}(\tilde{\nu})}{\rho_{40min}} \quad (2)$$

$$A^{norm}_{saturation}(\tilde{\nu}) = \sigma\left(\frac{A_{saturation_{40min}}(\tilde{\nu})}{\rho_{40min}} - \frac{A_{saturation_{8min}}(\tilde{\nu})}{\rho_{8min}}\right) \quad (3)$$

where $A_{operando_{40\ min}}(\tilde{\nu})$ are the final *operando* spectra recorded after 40 min of nanowire elongation (see Figure 3); $A_{saturation_{40\ min}}(\tilde{\nu})$ and $A_{saturation_{8\ min}}(\tilde{\nu})$ are the postgrowth saturation spectra recorded after cooling to room temperature in Ge_2H_6 following nanowire elongation for 40 and 8 min, respectively; ρ is the nanowire array areal density at the labeled elongation time (see Figure S2); and σ is a scaling factor that relates ν(Ge−H) intensity measured at nanowire growth temperature and room temperature. The second term in eq 3 prevents a systematic underestimate of θ_H. More specifically, the background spectrum of $A_{operando_{40\ min}}(\tilde{\nu})$ is collected during the initial 8 min of nanowire elongation, while the background spectrum of $A_{saturation_{40\ min}}(\tilde{\nu})$ is the H-free, Au-covered Ge substrate prior to initiating growth. Thus, if left uncorrected, this situation would lead to *operando* and postgrowth saturation measurements that probe different sidewall surface areas. We therefore require additional postgrowth saturation spectra, $A_{saturation_{8\ min}}(\tilde{\nu})$, recorded after 8 min of nanowire elongation at each condition. The morphology of these nanowires and the resulting spectra are shown in Figures S5 and S6, respectively.

Validating Sidewall Hydrogen Coverage Methodology. A series of control experiments validates the above methodology for determining the coverage of hydrogen atoms on the nanowire sidewall. Foremost, the Beer−Lambert law (i.e., the proportionality of resonator number and absorbance) must be valid for nanowire arrays. To prove that this is the case, despite the complex structure inherent in epitaxial nanowire arrays, we examine *operando* spectra recorded at different nanowire lengths for untapered growth at T_{sub} = 260 °C (i.e., where sidewall surface area linearly increases with time). Figure 4A confirms $I^{norm}_{operando}$ recorded at these growth conditions is linearly proportional to nanowire length, and hence number of resonators.

We also show that oscillator strength is unaffected by coverage and temperature at our synthesis conditions with *operando* measurements during Ge_2H_6 adsorption on vacuum-prepared, Au-free Ge(111) substrates (i.e., no nanowire growth). Figure 4B shows that ν(Ge−H) peak position remains constant at fixed T_{sub} and only integrated peak intensity increases with $p_{Ge_2H_6}$. The fixed peak position supports a ν(Ge−H) oscillator strength that is independent of surface coverage (i.e., weak interadsorbate interactions). The temperature dependence of the integrated peak intensity at a constant, saturation coverage is shown in Figure 4C. A subtle red-shift, but no dramatic change in integrated peak intensity, of the ν(Ge−H) mode is observed between T_{sub} = 260 and 305 °C. Therefore, we can conclude that processes such as adsorbate−phonon coupling[25,26] do not significantly impact oscillator strength over the narrow range of growth temperatures studied here. A saturation dose at T_{sub} = 330 °C was not attainable; however, the lack of peak broadening indicates the decrease in intensity is due to coverage.

It is also important to probe hydrogen adsorbed on the nanowire sidewall rather than the Ge(111) substrate. We orient

DOI: 10.1021/jacs.5b03818
J. Am. Chem. Soc. 2015, 137, 9861−9869

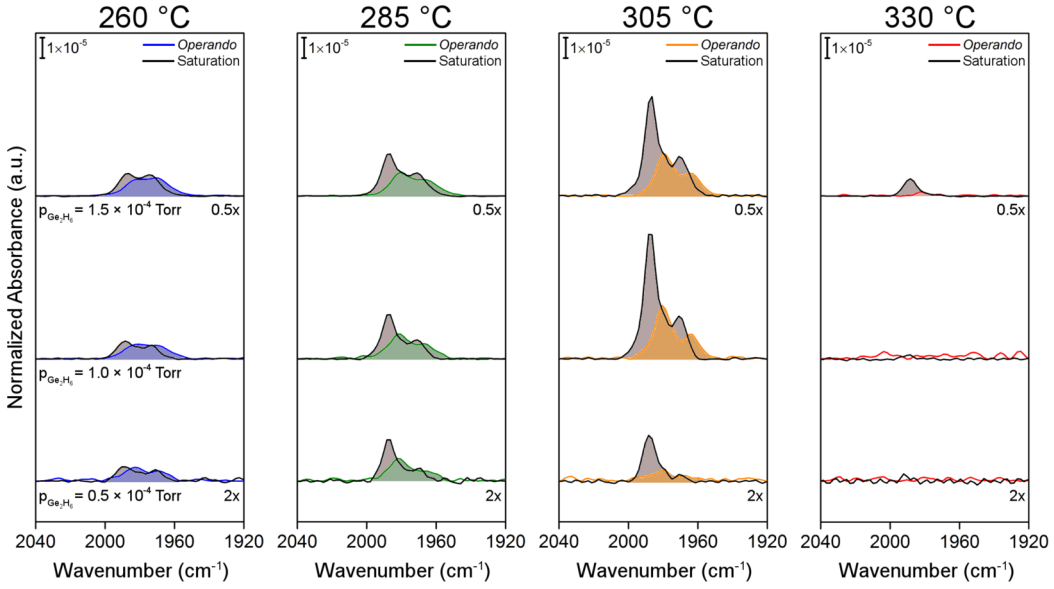

Figure 6. Comparison of *operando* and postgrowth measurements. Normalized *operando* and saturation infrared absorption spectra of the ν(Ge−H) stretching region for Ge nanowires grown at the indicated T_{sub} and $p_{Ge_2H_6}$. Spectra for $p_{Ge_2H_6}$ = 0.5 and 1.5 × 10^{-4} Torr are scaled by a factor of 2 and 0.5, respectively, for ease of comparison. Additional "high surface area" spectra for growth at T_{sub} = 330 °C are shown in Figure S7.

the Ge(111) substrate perpendicular to the infrared beam path during nanowire growth to prevent absorption from the solitary stretch of the Ge(111)-1×1:H surface. The planar *operando* experiment in Figure 4D confirms that ν(Ge−H) from the substrate is not detectable as a function of time at relevant growth conditions when the substrate is in this position. We note for comparison that strictly quantitative techniques for determining the number of hydrogen atoms bonded to the nanowire sidewall, such as temperature-programmed desorption, cannot discriminate between hydrogen atoms on the nanowire sidewall and those bonded to the Ge(111) substrate.

We determine the total number of surface sites on the nanowire by saturating the surface with hydrogen atoms upon cooling the substrate to room temperature in a Ge_2H_6 atmosphere. This requires that the final room temperature hydrogen coverage is the same upon cooling from all nanowire growth temperatures (T_{sub} = 260−330 °C) and that this coverage is unity. To show this, we expose vacuum-prepared, Au-free Ge(111) substrates to $p_{Ge_2H_6}$ = 1.0 × 10^{-4} Torr at various temperatures and then quench the substrate to room temperature at fixed $p_{Ge_2H_6}$. Figure 5A shows spectra recorded at the indicated T_{sub} and then after quenching to room temperature. Importantly, the same room temperature integrated peak intensity, and thus hydrogen coverage, is achieved for all starting temperatures. Upon cooling, facile Ge_2H_6 decomposition rapidly terminates the Ge surface with monohydride, precluding additional chemisorption of Ge_2H_6 and the observation of higher order hydrides. We note that the frequency of the ν(Ge−H) mode at room temperature, 1971 cm^{-1}, is identical to the work of Lu and Crowell.[24] Figure 5B shows that saturation exposures of Ge_2H_6 and atomic hydrogen at T_{sub} = 260 °C yield equivalent ν(Ge−H) integrated peak intensities, which indicates that Ge_2H_6 decomposition forms a complete hydrogen monolayer (i.e., one hydrogen per surface site) at our growth conditions.

The factor that accounts for differences in ν(Ge−H) absorption strengths between *operando* and postgrowth saturation spectra, σ, must also be determined. We calculate this value to be 0.86 by comparing a situation where hydrogen coverage is equivalent at elevated and room temperature. This occurs for a saturation dose of Ge_2H_6 at T_{sub} = 260 °C and the subsequent quench to room temperature in a Ge_2H_6 background (Figure 5A).

Correlating Nanowire Hydrogen Coverage with Growth Stability. A comparison of the relative integrated areas of $A^{norm}_{operando}(\tilde{\nu})$ and $A^{norm}_{saturation}(\tilde{\nu})$, as shown in Figure 6, provides a visual indication of θ_H as a function of T_{sub} and $p_{Ge_2H_6}$. For nanowires elongated at T_{sub} = 260 °C, corresponding to an untapered morphology (Figure 2), we see little peak area difference between the *operando* and saturation spectra. Sidewall taper increases from T_{sub} = 260 to 305 °C and is concomitant with increasingly distinct *operando* and saturation spectra. At the highest temperature, T_{sub} = 330 °C, ν(Ge−H) peaks are challenging to observe above the noise (Figure 3). To improve the signal-to-noise ratio at this temperature, we conduct a series of experiments (Figure S7) that begin with untapered nanowire growth, which serves to increase the overall nanowire surface area, and then transition to elongation at T_{sub} = 330 °C. We clearly resolve *operando* and saturation spectra at all $p_{Ge_2H_6}$ conditions and find significant deviations between them.

θ_H, plotted in Figure 7 as a function of T_{sub} and $p_{Ge_2H_6}$, strongly correlates with nanowire morphology and growth stability. At large θ_H values, nanowires exhibit almost no taper since hydrogen atoms impede Ge_2H_6 chemisorption on the sidewall. We observe increasing taper as θ_H decreases since Ge_2H_6 can now access the sidewall. Below a critical θ_H, stable nanowire growth is no longer possible. Importantly, θ_H supersedes T_{sub} and $p_{Ge_2H_6}$ as the best predictor of nanowire structure. For example, at T_{sub} = 260 or 285 °C, all partial pressures yield equivalent morphologies (Figure 2) and identical, within the error of our measurement, θ_H values (Figure 7). This relationship between θ_H and morphology also holds true at conditions where growth becomes unstable. Nanowires elongated at T_{sub} = 305 °C and $p_{Ge_2H_6}$ = 0.5 × 10^{-4}

DOI: 10.1021/jacs.5b03818
J. Am. Chem. Soc. 2015, 137, 9861−9869

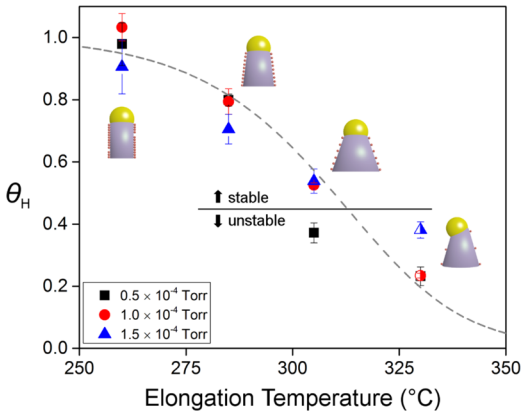

Figure 7. Effect of growth conditions on nanowire hydrogen coverage and growth stability. Nanowire sidewall surface hydrogen coverage, θ_H, as a function of T_{sub} and $p_{Ge_2H_6}$. Filled and half-filled shapes represent coverages determined from spectra shown in Figures 6 and S7, respectively. Gray dashed line is a fit to a kinetic model that includes Ge_2H_6 adsorption and H_2 desorption.

Torr and T_{sub} = 330 °C and $p_{Ge_2H_6}$ = 1.5 × 10^{-4} Torr share a common θ_H and a strikingly similar morphology.

The value of θ_H for a given set of conditions can be understood with a simple Langmuirian kinetic model that includes dissociative Ge_2H_6 adsorption and H_2 desorption (see Kinetic Model in Supporting Information). At low T_{sub}, θ_H is high because the rate of H_2 desorption is slow relative to Ge_2H_6 adsorption. Thus, we do not observe a dependence of θ_H on $p_{Ge_2H_6}$ between T_{sub} = 260 and 285 °C. At these conditions, variability in θ_H likely arises from the diversity of sidewall surface sites, possessing slightly different hydrogen desorption rates.[23,27] As T_{sub} increases, θ_H begins to decrease as H_2 desorption exponentially accelerates, and θ_H becomes increasingly dependent on Ge_2H_6 impingement rate. Our kinetic model captures the essence of θ_H variations as a function of growth parameters but deviates from the experimental θ_H values at low coverage, likely due to the transition between first and second order desorption kinetics.[23]

Surpassing the Hydride Limit. We adsorb an alternative functionality, methyl groups, on the nanowire sidewall that maintains stable nanowire growth beyond the desorption temperature of H_2 and circumvents a fundamental limitation of conventional hydride precursors. Figure 8A shows the morphology of nanowires grown first with Ge_2H_6 for 32 min, which generates a tapered base, and then with Ge_2H_6 and GeH_3CH_3 coflow. The *operando* spectrum collected after 32 min, as seen in Figure 8B,C, indicates that only hydrogen atoms exist on the nanowire sidewall prior to GeH_3CH_3 introduction. Upon addition of GeH_3CH_3 at T_{sub} = 305 °C, Figure 8B exhibits an absorption peak in the ν(C−H) stretching region. This peak, positioned at 2899 cm^{-1}, is consistent with methyl groups bonded to a Ge surface[28] at elevated temperature. As seen in Figure 8C, the ν(Ge−H) bands redshift upon GeH_3CH_3 addition, as expected for mixed monolayers.[29] While continuing Ge_2H_6 and GeH_3CH_3 flow, we then raise the temperature to T_{sub} = 330 °C, where stable growth is not possible with Ge_2H_6 alone, for an additional 32 min. Figure 8A confirms that growth remains stable and the yield of ⟨111⟩ oriented nanowires is near 100%. The intensity of the ν(C−H)

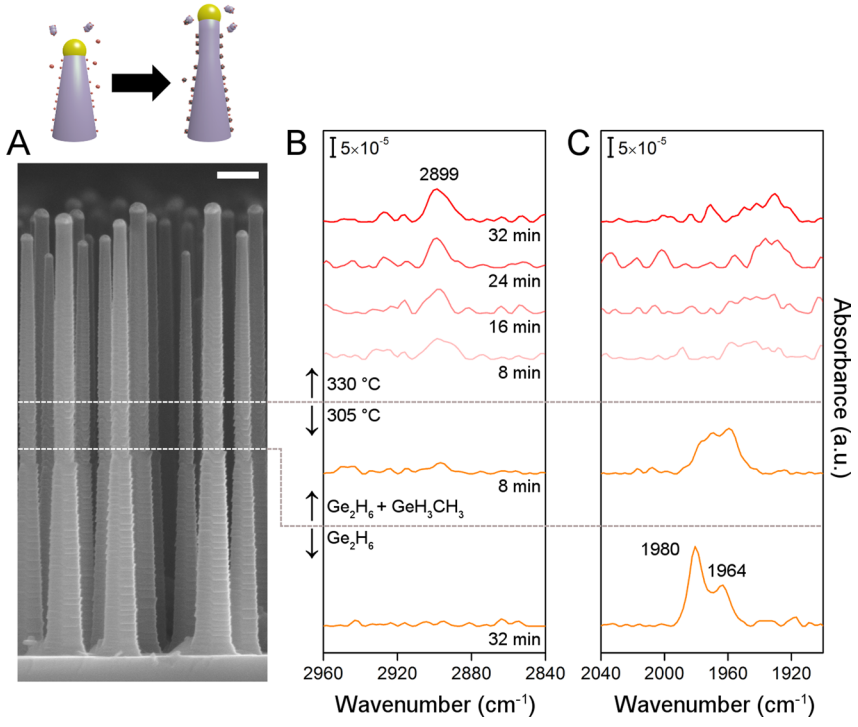

Figure 8. Influence of GeH_3CH_3 sidewall adsorption on nanowire growth stability. (A) Representative side-view SEM image of Ge nanowires initially elongated at T_{sub} = 305 °C and $p_{Ge_2H_6}$ = 1 × 10^{-4} Torr for 32 min prior to GeH_3CH_3 introduction at $p_{GeH_3CH_3}$ = 1 × 10^{-4} Torr. After 8 min of elongation with Ge_2H_6 and GeH_3CH_3 coflow, the substrate temperature is raised to T_{sub} = 330 °C and growth continues for an additional 32 min. Scale bar, 200 nm. Illustration depicts a tapered nanowire before and after introduction of GeH_3CH_3. *Operando* infrared absorption spectra of (B) ν(C−H) and (C) ν(Ge−H) stretching regions, respectively. All spectra are referenced to the first 8 min of nanowire elongation at T_{sub} = 305 °C.

DOI: 10.1021/jacs.5b03818
J. Am. Chem. Soc. 2015, 137, 9861−9869

mode increases during elongation at T_{sub} = 330 °C and indicates reasonably long methyl lifetimes.

DISCUSSION AND CONCLUSIONS

Our experiments highlight the influence of solid−vapor interface chemistry during nanowire growth, and a number of considerations support its central role for the Au/Ge system. Foremost, the observed morphological changes and ultimate onset of growth instability occur over a narrow temperature range and are consistent with kinetic processes, here H_2 desorption from the sidewall. Changes in the liquid−solid (γ_{LS}) and liquid−vapor (γ_{LV}) interfacial energies, which can also influence catalyst behavior,[30] are not expected to be large over this temperature range. Indeed, for the Au−Ge alloy, γ_{LV} is a weak function of temperature and varies only by a few percent over hundreds of degrees.[31] While surface bonding can reduce γ_{LV},[32] hydrogen desorbs from Au surfaces well below room temperature.[33] If hydrogen were bonded to Ge atoms segregated to the liquid−vapor interface, increasing temperature would yield a lower hydrogen coverage, thus increasing γ_{LV} and stabilizing the catalyst (i.e., acting opposite to our observation). No significant variations in γ_{LS} are expected since catalyst composition does not change appreciably over this narrow temperature range and nanowire crystal structure remains diamond cubic.

We offer two plausible explanations for the observed growth destabilization when θ_H is low. In the first scenario, as originally predicted by Nebol'sin and Shchetinin,[30] the solid−vapor interface energy (γ_{SV}) increases with decreasing θ_H until the catalyst droplet can no longer be supported atop the nanowire. While the intrinsic surface energy of a solid is specific to the material and cleavage plane,[34] it is well known that adsorbates can substantially reduce the surface free energy.[35] The difference in γ_{SV} between a bare and hydrogen-passivated Ge(111) surface, for example, is calculated to be ∼1.4 J/m^2.[36] Here, the reduction of θ_H increases γ_{SV} and results in a loss of droplet stability. In the alternative scenario, hydrogen atoms bonded to the nanowire prevent diffusion of Au or Ge atoms from the catalyst to the sidewall. This enables large supersaturations and maintains a metastable AuGe liquid below the bulk eutectic temperature.[19] Below a threshold θ_H, the droplet solidifies and sub-eutectic VLS growth ceases. Further studies are required to determine whether the destabilization observed here can be explained by one, if either, of these scenarios.

Our study, irrespective of the ultimate catalyst destabilization mechanism, has a number of implications for understanding and controlling nanowire morphology. Foremost, these findings argue against the use of a constant value for γ_{SV} when modeling nanowire growth and suggest a reevaluation of these models for situations where surface chemistry may be rapidly changing.[37] We show how growth stability and morphology are strongly coupled when using a single, conventional hydride precursor. This interdependency can be broken by independently delivering distinct surface species (e.g., methyl groups) to the sidewall, creating new opportunities to control and enhance the diversity of nanowire structure. Notably, the observation of both hydrogen and methyl on the nanowire sidewall suggests that the chemical vapor deposition growth of compound semiconductor nanowires, which usually employs a mixture of organometallic and hydride species, may be impacted by similar processes.

These experiments also provide insight into, and propose possible solutions for, long-standing challenges in catalyst selection, heterostructure formation, and impurity doping. Many of the alternative catalyst materials, particularly those with optoelectronic properties more favorable than Au, result in poor growth morphologies or limited growth stability.[38] Our work indicates that sidewall-stabilizing species, delivered in conjunction with traditional hydrides, offer renewed prospects for many previously rejected catalyst materials. Analogous surface species are also expected to mitigate the undesirable morphologies often observed during heterostructure formation.[39] Poor morphologies likely result, at least partially, from differences in sidewall adsorption and desorption rates upon wholesale changes to precursor chemistry.[40] Perfect control of dopant profile with hydrides alone is also unlikely due to the dynamics of adsorption and desorption. Even at conditions favoring a high time-averaged hydrogen surface coverage and minimal sidewall taper, traditional dopant precursors (e.g., PH_3) can access the sidewall during the finite time after an H_2 desorption event and before subsequent precursor (e.g., Ge_2H_6) adsorption.[11] The tailoring of dopant precursor ligands[41] or use of longer-lived sidewall species promises to reduce unintended radial doping and increase the selectivity of decomposition at the catalyst. The fundamental chemical knowledge provided here promises to advance the rational synthetic design of nanowire structure and function.

EXPERIMENTAL SECTION

Chamber Setup. All measurements are completed in a custom-built ultra-high-vacuum (UHV) chamber with a base pressure of 3 × 10^{-10} Torr (McAllister Technical Services). A schematic of the experimental setup is shown in Figure S1. Substrate heating is accomplished resistively. Substrate temperature is monitored by an infrared pyrometer (Mikron) focused on the backside of the substrate. The pyrometer is calibrated with two methods: temperature-programmed desorption of H_2 from a Ge(100)-2×1 surface and by bonding a Type K thermocouple to the center of the substrate. Chamber pressure is monitored with a nude ion gauge. Pressures are not corrected for ion gauge sensitivity. A thermal evaporator (SVT Associates) is used to deposit Au (ESPI Metals, 99.999%) onto the substrate. Film thickness is monitored by a bakeable quartz crystal microbalance (Inficon). Differentially pumped KBr windows (ISP Optics) enable infrared light input and output. Two variable leak valve and stainless doser combinations permit separate delivery of Ge_2H_6 (Voltaix, 20% in He) and GeH_3CH_3 (Gelest, 97%). Both species are used without further purification. A tungsten filament, located ∼15 cm from the substrate, enables atomic hydrogen delivery via H_2 cracking.

Substrate Preparation. Substrates (6 mm × 24 mm) are cut from nominally undoped, double-side polished Ge(111) (MTI Corp., CZ, 500 μm, 42−64 Ω-cm) or Ge(100) (MTI Corp., CZ, 500 μm, >45 Ω-cm) wafers. Each substrate is chemically cleaned using the oxidation and strip procedure described by Han et al.[25] Immersion of the substrate in 3 wt % H_2O_2 (JT Baker, 30 wt %, ACS grade) for 1 min forms an oxide, which is subsequently stripped for 30 s with 9 wt % HCl (JT Baker, CMOS grade). The substrate is rinsed with deionized (DI) water and dried with N_2 gas (Airgas, 99.999%) between each step. After multiple oxidation and strip cycles, immersion of the substrate in a 1:2:20 NH_4OH (Sigma-Aldrich, 28−30 wt %, ACS grade):H_2O_2:H_2O solution for 1 min grows a final oxide. The substrate is rinsed again with DI water and dried with N_2. Upon insertion into the UHV chamber, the sample is heated to T_{sub} = 485 °C for 35 min to desorb the previously grown oxide. An epitaxial Ge thin film is then deposited at T_{sub} = 305 °C and $p_{Ge_2H_6}$ = 2 × 10^{-5} Torr.

Nanowire Synthesis. A thin layer (<0.5 nm) of Au is evaporated onto the Ge(111) substrate. Nanowire synthesis begins with the substrate oriented 58° relative to the beam path and facing the Ge_2H_6 doser. All Ge nanowires are grown via a two-step protocol, illustrated in Figure S3, which consists of incubation and elongation steps. The

DOI: 10.1021/jacs.5b03818
J. Am. Chem. Soc. 2015, 137, 9861−9869

incubation step begins with Ge_2H_6 introduction at $p_{Ge_2H_6} = 2 \times 10^{-6}$ Torr. To suppress island formation,[42] GeH_3CH_3 is also added through a separate leak valve at $p_{GeH_3CH_3} = 1 \times 10^{-5}$ Torr and the substrate is then heated to T_{sub} = 485 °C at a rate of 10 K/s. The substrate temperature is held for 30 s, then cooled to T_{sub} = 305 °C at a rate of 3 K/s, at which time GeH_3CH_3 flow is terminated. The Ge_2H_6 partial pressure is then increased to $p_{Ge_2H_6} = 1 \times 10^{-4}$ Torr and held for 5 min to grow the short nanowires shown in Figure S3E and F. The elongation step is initiated, while maintaining Ge_2H_6 flow, by rotating the substrate such that the nanowire long axes are perpendicular to the incoming infrared beam. Elongation then occurs at the substrate temperatures (T_{sub} = 260−330 °C) and Ge_2H_6 partial pressures ($p_{Ge_2H_6}$ = (0.5−1.5) × 10^{-4} Torr) indicated in the main text.

Infrared Spectroscopy. A Fourier transform infrared (FTIR) spectrometer (Bruker, Vertex 70) equipped with a narrow-band liquid N_2-cooled HgCdTe (MCT) detector is coupled to the above-described vacuum chamber and used to measure the vibrational modes of surface adsorbates. All measurements utilize unpolarized light and a spectrometer resolution of 4 cm^{-1}. Each *operando* spectrum consists of 2000 scans and is referenced to the *operando* spectrum collected during the initial 8 min of elongation. Each postgrowth saturation spectrum consists of 512 scans and is referenced to a H-free, Au-covered Ge substrate at room temperature. All nanowire spectra are recorded with the substrate oriented perpendicular to the beam path. Spectra from planar adsorption studies are collected as indicated in each figure caption. All spectra are baseline-corrected using a standard concave rubber band method.

Electron Microscopy. Nanowire morphology is examined with a Zeiss Ultra60 field emission scanning electron microscope (SEM) and a FEI Titan S 80-300 aberration-corrected transmission electron microscope (TEM). Nanowires are removed from the growth substrate via sonication in methanol (BDH, ACS grade) prior to drop-casting onto lacey carbon grids (Ted Pella).

■ ASSOCIATED CONTENT

Supporting Information

Kinetic model and additional figures. The Supporting Information is available free of charge on the ACS Publications website at DOI: 10.1021/jacs.5b03818.

■ AUTHOR INFORMATION

Corresponding Author

*michael.filler@chbe.gatech.edu

Present Address

†Department of Chemical Engineering, Inha University, Incheon 402-751, Republic of Korea.

Notes

The authors declare no competing financial interest.

■ ACKNOWLEDGMENTS

The authors acknowledge support from the National Science Foundation (#1133563 and #1150755) and Camille and Henry Dreyfus Postdoctoral Program in Environmental Chemistry. S.V.S. gratefully acknowledges support from a NSF IGERT fellowship (#1069138). Research was supported by ORNL's Shared Research Equipment (ShaRE) User Program, which is sponsored by the Office of Basic Energy Sciences, the U.S. Department of Energy. We thank Athanasios Nenes and Sankar Nair for their careful critique of our manuscript. This work would not have been possible without support from the staff at the Georgia Tech Institute for Electronics and Nanotechnology (IEN). Discussions with Ye Xu, Phani Dathar, Ho Yee Hui, and Ildar Musin were fruitful and appreciated.

■ REFERENCES

(1) Krogstrup, P.; Jorgensen, H. I.; Heiss, M.; Demichel, O.; Holm, J. V.; Aagesen, M.; Nygard, J.; Morral, A. F. I. *Nat. Photonics* **2013**, *7*, 306.
(2) Pribiag, V. S.; Nadj-Perge, S.; Frolov, S. M.; van den Berg, J. W.; van Weperen, I.; Plissard, S. R.; Bakkers, E. P.; Kouwenhoven, L. P. *Nat. Nanotechnol.* **2013**, *8*, 170.
(3) Duan, X.; Huang, Y.; Agarwal, R.; Lieber, C. M. *Nature* **2003**, *421*, 241.
(4) Kempa, T. J.; Tian, B. Z.; Kim, D. R.; Hu, J. S.; Zheng, X. L.; Lieber, C. M. *Nano Lett.* **2008**, *8*, 3456.
(5) Gudiksen, M. S.; Lauhon, L. J.; Wang, J.; Smith, D. C.; Lieber, C. M. *Nature* **2002**, *415*, 617.
(6) Algra, R. E.; Verheijen, M. A.; Borgstrom, M. T.; Feiner, L. F.; Immink, G.; van Enckevort, W. J. P.; Vlieg, E.; Bakkers, E. *Nature* **2008**, *456*, 369.
(7) Dayeh, S. A.; Mack, N. H.; Huang, J. Y.; Picraux, S. T. *Appl. Phys. Lett.* **2011**, *99*, 023102.
(8) Brewster, M. M.; Zhou, X. A.; Lim, S. K.; Gradecak, S. *J. Phys. Chem. Lett.* **2011**, *2*, 586.
(9) Kolíbal, M.; Vystavěl, T.; Varga, P.; Šikola, T. *Nano Lett.* **2014**, *14*, 1756.
(10) Xie, P.; Hu, Y. J.; Fang, Y.; Huang, J. L.; Lieber, C. M. *Proc. Natl. Acad. Sci. U. S. A.* **2009**, *106*, 15254.
(11) Perea, D. E.; Hemesath, E. R.; Schwalbach, E. J.; Lensch-Falk, J. L.; Voorhees, P. W.; Lauhon, L. J. *Nat. Nanotechnol.* **2009**, *4*, 315.
(12) Hillerich, K.; Dick, K. A.; Wen, C.-Y.; Reuter, M. C.; Kodambaka, S.; Ross, F. M. *Nano Lett.* **2013**, *13*, 903.
(13) Dayeh, S. A.; Wang, J.; Li, N.; Huang, J. Y.; Gin, A. V.; Picraux, S. T. *Nano Lett.* **2011**, *11*, 4200.
(14) Shin, N.; Filler, M. A. *Nano Lett.* **2012**, *12*, 2865.
(15) Kodambaka, S.; Hannon, J. B.; Tromp, R. M.; Ross, F. M. *Nano Lett.* **2006**, *6*, 1292.
(16) Yang, Z.-X.; Han, N.; Fang, M.; Lin, H.; Cheung, H.-Y.; Yip, S.; Wang, E.-J.; Hung, T.; Wong, C.-Y.; Ho, J. C. *Nat. Commun.* **2014**, *5*, 5249.
(17) Greenlief, C. M.; Armstrong, M. *J. Vac. Sci. Technol., B: Microelectron. Process. Phenom.* **1995**, *13*, 1810.
(18) Kodambaka, S.; Tersoff, J.; Reuter, M. C.; Ross, F. M. *Phys. Rev. Lett.* **2006**, *96*, 096105.
(19) Kodambaka, S.; Tersoff, J.; Reuter, M. C.; Ross, F. M. *Science* **2007**, *316*, 729.
(20) Oh, S. H.; Chisholm, M. F.; Kauffmann, Y.; Kaplan, W. D.; Luo, W.; Rühle, M.; Scheu, C. *Science* **2010**, *330*, 489.
(21) Gamalski, A. D.; Ducati, C.; Hofmann, S. *J. Phys. Chem. C* **2011**, *115*, 4413.
(22) Chou, Y. C.; Hillerich, K.; Tersoff, J.; Reuter, M. C.; Dick, K. A.; Ross, F. M. *Science* **2014**, *343*, 281.
(23) Lee, J. Y.; Maeng, J. Y.; Kim, A.; Cho, Y. E.; Kim, S. *J. Chem. Phys.* **2003**, *118*, 1929.
(24) Lu, G. Q.; Crowell, J. E. *J. Chem. Phys.* **1993**, *98*, 3415.
(25) Han, X.; Balgar, T.; Hasselbrink, E. *J. Chem. Phys.* **2009**, *130*, 134701.
(26) Dumas, P.; Chabal, Y. J.; Higashi, G. S. *Phys. Rev. Lett.* **1990**, *65*, 1124.
(27) Kim, H.; Vailionis, A.; Cahill, D. G.; Greene, J. E. *Surf. Sci.* **2000**, *457*, 337.
(28) Knapp, D.; Brunschwig, B. S.; Lewis, N. S. *J. Phys. Chem. C* **2011**, *115*, 16389.
(29) Filler, M. A.; Van Deventer, J. A.; Keung, A. J.; Bent, S. F. *J. Am. Chem. Soc.* **2006**, *128*, 770.
(30) Nebol'sin, V. A.; Shchetinin, A. A. *Inorg. Mater.* **2003**, *39*, 899.
(31) Naidich, Y. V.; Perevertailo, V. M.; Obushchak, L. P. *Powder Metall. Met. Ceram.* **1975**, *14*, 403.
(32) Ricci, E.; Arato, E.; Passerone, A.; Costa, P. *Adv. Colloid Interface Sci.* **2005**, *117*, 15.
(33) Stobiński, L.; Duś, R. *Surf. Sci.* **1992**, *269/270*, 383.
(34) Jaccodine, R. J. *J. Electrochem. Soc.* **1963**, *110*, 524.
(35) Somorjai, G. A.; Van Hove, M. A. *Prog. Surf. Sci.* **1989**, *30*, 201.

DOI: 10.1021/jacs.5b03818
J. Am. Chem. Soc. 2015, 137, 9861−9869

(36) Zhang, S. B.; Wei, S.-H. *Phys. Rev. Lett.* **2004**, *92*, 086102.
(37) Shakthivel, D.; Raghavan, S. *J. Appl. Phys.* **2012**, *112*, 024317.
(38) Schmidt, V.; Wittemann, J. V.; Gosele, U. *Chem. Rev.* **2010**, *110*, 361.
(39) Dick, K. A.; Kodambaka, S.; Reuter, M. C.; Deppert, K.; Samuelson, L.; Seifert, W.; Wallenberg, L. R.; Ross, F. M. *Nano Lett.* **2007**, *7*, 1817.
(40) Ning, B. M. H.; Crowell, J. E. *Surf. Sci.* **1993**, *295*, 79.
(41) Lew, K.-K.; Pan, L.; Bogart, T. E.; Dilts, S. M.; Dickey, E. C.; Redwing, J. M.; Wang, Y.; Cabassi, M.; Mayer, T. S.; Novak, S. W. *Appl. Phys. Lett.* **2004**, *85*, 3101.
(42) Bramblett, T. R.; Lu, Q.; Lee, N. E.; Taylor, N.; Hasan, M. A.; Greene, J. E. *J. Appl. Phys.* **1995**, *77*, 1504.
(43) Dick, D.; Veyan, J.-F.; Longo, R. C.; McDonnell, S.; Ballard, J. B.; Qin, X.; Dong, H.; Owen, J. H. G.; Randall, J. N.; Wallace, R. M.; Cho, K.; Chabal, Y. J. *J. Phys. Chem. C* **2014**, *118*, 482.

DOI: 10.1021/jacs.5b03818
J. Am. Chem. Soc. 2015, 137, 9861−9869